Crustal resistivity structure of the Lunpola basin in central Tibet and its tectonic implications

Shuai Xue[1], Zhanwu Lu[1*], Wenhui Li[1], Haiyan Wang [1]

[1] Key Laboratory of Deep-Earth Dynamics of Ministry of Natural Resources, Institute of Geology, Chinese Academy of Geological Sciences, Beijing 100037, China.

Corresponding author: Zhanwu Lu (luzhanwu78@163.com)

Key Points:

- Magnetotelluric data are collected across the Lunpola basin in central Tibet;
- 3-D magnetoteluric inversion result shows the significant low-resistivity mid-to-lower crust beneath the Lunpola basin;
- The less-well-developed weak mid-to-lower crust in central Tibet escapes eastward in a rigid block fashion.

Abstract

In the central Tibetan Plateau, an east-west trending band of basins is developed. How such topography formed and the underlying geodynamic processes are still in debate. Magnetotelluric data were collected across the Lunpola basin to study the crustal structure beneath central Tibet. Phase tensors and 3-D inversion are employed to obtain the electrical resistivity model. Our model clearly portrays conductive sedimentary layers beneath the basins with average resistivity of 2.0 Ω·m. The low-resistivity mid-to-lower crust is revealed beneath the Lunpola basin with bulk resistivity of 20 Ω·m and fluid fraction of 1.3-3.0%, which would be attributed to partial melting. Compared to the significant conductive crust in southern Tibet, the crustal rheology is less well developed beneath central Tibet. We propose that the asthenospheric flow beneath central Tibet is responsible for the crustal partial melting and drives the eastward escape of the continental lithosphere in a rigid block fashion.

Plain Language Summary

The Lunpola basin, belonging to the east-west trending band of basins in the central Tibetan Plateau, records the evolution history of Tibetan Plateau and has good potential in oil and gas resources. Compared to the rugged terrain in southern Tibet, the high-elevation low-relief landform in central Tibet is formed and is less studied. In order to understand the formation of the basins and the underlying geodynamic processes, we utilize magnetotelluric data collected across the Lunpola basin to obtain the deep electrical resistivity structure. The thick sediments beneath the Lunpola basin is clearly imaged with conductive layers. We find that the Lunpola basin has low-resistivity mid-to-lower crust which would be attributed to partial melting. This conductive mid-to-lower crust beneath the central Tibet indicates a less-well-developed rheologically weak state, and is different from the crustal structures beneath the southern Tibet

where anomalously conductive layers in mid-to-lower crust are ubiquitously developed. Combined with previous results, we suggest the weak crust beneath the Lunpola basin is blamed for heating from the hot upwelling asthenosphere, and the eastward escape of the wedge basins bounded by conjugate strike-slip faults in central Tibet is driven by the asthenospheric flow in a rigid block fashion.

1 Introduction

The collision and convergence between the Indian and Asian plates result in the significant N-S shortening, eastward escape and vertical crustal thickening of the Tibetan Plateau, which form largest and highest plateau with abundant active thrust, normal and strike-slip faults on earth (Armijo et al., 1989; Yin et al., 2000, 2011; Tapponnier et al., 2001; Kapp et al., 2005). However, how such topography formed and the crust deformed is still in debate. In central Tibet, an east-west trending band of basins accompanied with a series of V-shaped conjugate strike-slip faults is developed along the Bangong-Nujiang Suture Zone (BNSZ) formed by the Mesozoic collision of the Lhasa and Qiangtang terranes (Yin et al., 2000, 2011; Tapponnier et al., 2001) (Fig.1), and spans most of the interval covering the collision of India and Asia and the resulting tectonic deformation and plateau growth (Rowley and Currie, 2006; Fang et al., 2020; Xiong et al., 2022). Recently, these basins have been the focus to understanding Tibetan elevation evolution and study geodynamic mechanism of the continental deformation (Rowley and Currie, 2006; Wu et al., 2016; Su et al., 2019; Fang et al., 2020; Xiong et al., 2022).

The Lunpola basin, one of the several depositional centers in central Tibet, records the most complete Cenozoic sedimentary history (Wu et al., 2016; Su et al., 2019; Fang et al., 2020; Xiong et al., 2022). The palaeo-environment and palaeo-elevation estimations derived from the Lunpola basin support the elevations of central Tibet were generally low (<2.3 km) in the Eocene and became high (>~4 km) since the early Miocene (Su et al., 2019; Fang et al., 2020; Xiong et al., 2022). The formation of the basin would be attributed to the rejuvenation of the BNSZ and the development of the V-shaped conjugate strike-slip faults in response to far-field compression of the India-Asia collision (Kapp et al., 2005; Wang et al., 2014). The central Tibet conjugate strike-slip faults are kinematically linked north trending Tibetan rifts located north and south of the conjugate fault systems. The conjugate strike-slip faults together with the Tibetan rifts facilitate coeval north-south contraction and east-west extension accommodated by the eastward extrusion of a series of small wedges bounded by these conjugate strike-slip faults (Armijo et al., 1989; Tapponnier et al., 2001).

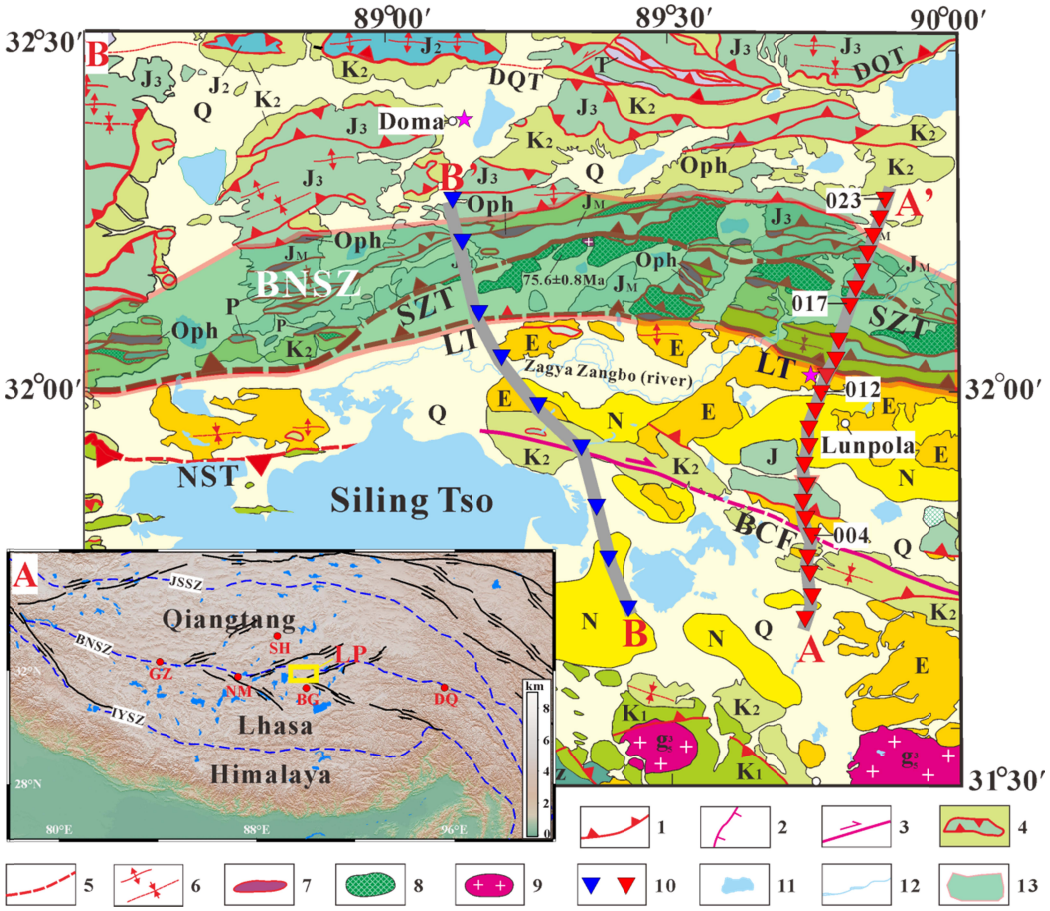

Figure 1. Topographic and geological maps showing the location of the Lunpola region and the MT sites. (A) Topography of the Tibetan Plateau and neighboring regions illustrating the main tectonic boundaries (blue dashed lines), a series of the Cenozoic Tibetan Valley (red circles), the location of the Lunpola Basin (yellow rectangle), and other faults. (B) Geologic map of the Lunpola basin and the location of the MT sites (red and blue triangles). Abbreviations in Fig. 1A: GZ, Gerze Basin; NM, Nima basin; SH, Shuanghu Basin; BG, Bangor Basin; DQ, Dingqing Baisn; LP, Lunpola Basin; JSSZ, Jinsha Suture Zone; BNSZ, Bangong-Nujiang Suture Zone; IYSZ, Indus-Yarlung Suture Zone. Abbreviations in Fig. 1B: BCF, Bengco strike-slip fault; NST, Nima-Silingco thrust; LT, Lunpola thrust; SZT, Saibuco-Zagya thrust; DQT, Doma-Qixiangco thrust. 1-Thrust fault; 2-normal fault; 3-strike-slip fault; 4-nappe; 5-covered fault; 6-folds; 7-ophiolite; 8-Late Cretaceous volcanic rocks; 9-granite; 10-MT sites; 11-lake; 12-river; 13-Bangong-Nujiang Suture Zone. Q-Quaternary mud, sands and gravel; N-Neogene sedimentary rocks; E-Paleogene lacustrine, fluvial, and alluvial mudstone, sandstone, marl and conglomerate; K_2-Upper Cretaceous red-beds; K_2-Lower Cretaceous limestone and clastic sedimentary rocks; J_3-Upper Jurassic limestone; J_2-Middle Jurassic limestone, dolomite, sandstone, siltstone and shale; J_1-Lower Jurassic sandstone, siltstone, shale and mudstone; J_M-Jurassic mélange; T-Triassic system; P-Permian; Oph-ophiolite; magenta stars represent the heat ; The gray lines AA' and BB' refer to MT profile.

In this study, we mainly used MT data collected along a relatively densely spaced array (~3 km) across the Lunpola basin and nearby area to obtain a 3-D resistivity model for the basin. These MT data allow us to reveal and define crustal structures beneath the basin in central Tibet. From the resistivity model, we analyse and discuss the characteristics of the upper and mid-to-lower crust, calculate the conductance in the depth range of 30-60 km, and alternative geodynamic processes.

2 Regional geological setting

The high-elevation low-relief landform along the BNSZ in central Tibet, extends east-west over a distance of ~1500 km with 20-100 km wide in a north-south direction, including the Gerze Basin in the west, the Bangor, Lunpola, and Nima Basins in the middle and the Dingqing Basin in the east (Fig. 1A). The Lunpola basin is approximately bounded by the Bengco strike-slip fault (BCF) to the south and the BNSZ to the north (Fig.1B). The Lunpola basin contains 4-5 km thick sequences of lacustrine to alluvial sediments, which is believed to have been deposited in a compressional tectonic background initiated in the Late Cretaceous-Early Eocene and reactivated by thrusting in the Early Miocene (Kapp et al., 2005; Wang et al., 2014; Fang et al., 2020). The Cenozoic strata of the Lunpola basin consist of two primary stratigraphic units: the Palaeocene-Oligocene Niubao Formation and the Miocene-Pliocene Dingqing Formation (Rowley and Currie, 2006; Wu et al., 2016; Xiong et al., 2022). The Niubao formation is mainly composed of conglomerates, sandstones, mudstones, marls and tuffs (Wu et al., 2016; Xiong et al., 2022) (Fig. 1B). The Dingqing formation mainly consists of mudstones, shales, sandstones, siltstones and tuffite layers (Wu et al., 2016; Xiong et al., 2022) (Fig. 1B). The depositional ages of the Niubao Formation and the Dingqing Formation are constrained to ~50-29 Ma and ~29-20 Ma respectively (Wang et al., 2014; Wu et al., 2016; Fang et al., 2020).

3 Data acquisition, processing and inversion

3.1 Data acquisition

In 2022, MT data were collected at 23 sites along a nearly N-S transect AA' which is approximately orthogonal to the regional strike of tectonics (red triangles in Fig. 1B). With sites spaced ~3.0 km, the total length of transect AA' was ~70 km. Five components of the time-varying electromagnetic field (Ex, Ey, Hx, Hy, Hz) were measured using commercial Phoenix MTU-5A instruments. The time series were analyzed and processed through robust statistic methods (Egbert, 1997) to estimate MT impedances for the period range of ~0.01-1000 s. Because of sparsely population and poor industries in central Tibet, the quality of the acquired MT data was generally good (Fig. 2). Besides, to the west of the MT profile AA', previous MT data of 9 sites with average ~10 km separation along the profile BB' (blue triangles in Fig. 1B) were supplementary to this study (Liang et al., 2018; Xue et al., 2022).

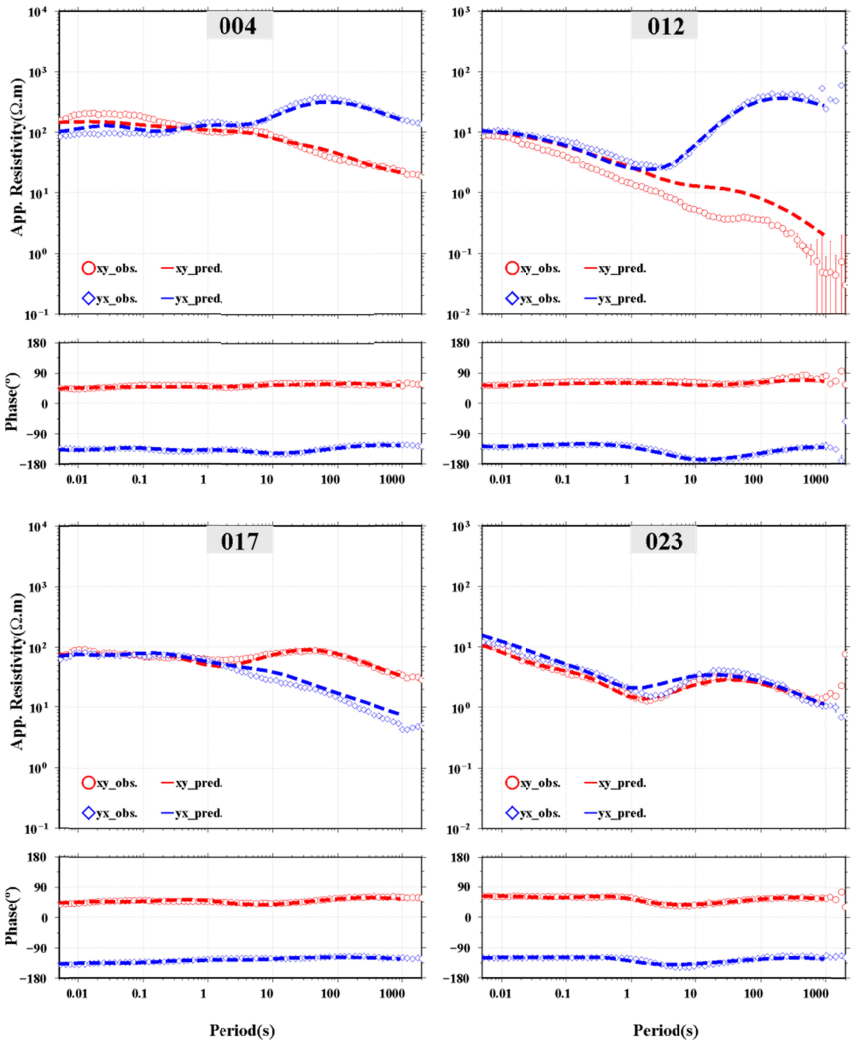

Figure 2. Examples of MT apparent resistivity and phase curves along the profile AA' (locations of sites 004, 012, 017 and 023 are illustrated in Fig. 1b). The red circles and blue rhombuses represent the off-diagonal elements of the impedances. The broken lines (red and blue) show the predicated responses for the preferred model. The error bars are corresponding to the measurement errors of the observed data.

3.2 Phase Tensor analysis

Before the inversion and interpretation of magnetotelluric data are carried out, the phase tensor (PT) decomposition method (Caldwell et al., 2004) is employed to evaluate the dimensionality of the subsurface structure for judging whether a 2D or 3D approach is more appropriate. MT phase tensors are generally expressed as a series of ellipses. The orientations of major axis of the PT ellipses indicate the PT strike direction. The PT skew angle β is represented by the color fills of the ellipse and denotes dimensionality at different periods. Generally, $\beta<3°$ is required for the data to satisfy 1-D or 2-D assumptions (Booker, 2014; Xue et al., 2021, 2022).

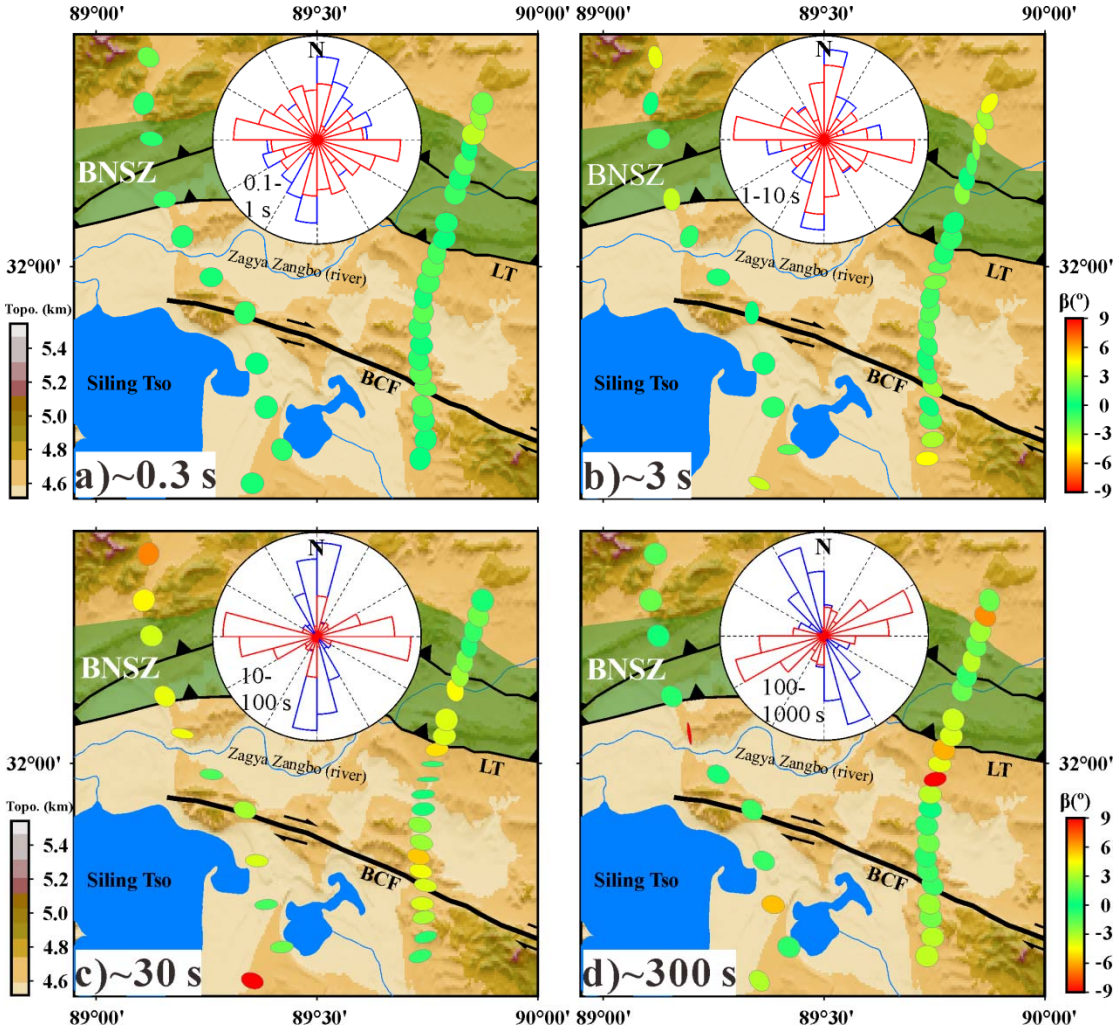

Figure 3. The phase tensor (PT) ellipses for periods: (a) 0.3 s, (b) 3 s, (c) 30 s, (d) 300 s. Rose diagrams show PT strike analysis results for each corresponding period band (0.1-1 s, 1-10 s, 10-100 s, 100-1000 s).

The PT ellipses for each of the 32 sites were plotted in the four periods (~0.3 s, 3.0 s, 30.0 s, 300.0 s) and the rose diagrams of PT strike directions were summarized statistically in the four period bands (0.1-1.0 s, 1.0-10.0 s, 10.0-100.0 s, 100.0-1000.0 s) shown both in Figure 3. At periods 0.3 s and 3.0 s, the PT analysis with small skew angles suggests 1-D or 2D dimensionality at most sites (Fig. 3a and b). The PT strike directions in period bands 0.1-1.0 s and 1.0-10.0 s (Fig. 3a and b) show that a strike direction in the range east to N105°E is the preferred for these data (or orthogonal directions). As period increases to 30.0 s and 300.0 s (Fig. 3c and d), multiple PT skew angles near the BNSZ and BCF rise over 3° without any clear consistent strike directions. For the period band 10.0 -100.0 s, the predominant strike direction clearly lies between east and N105°E with a secondary preferred strike direction between N75°E and east (Fig. 3c). However, the preferred strike direction changes into the range of N60°E-N75°E with a secondary preferred direction between N75°E and east for the period band 100.0-1000.0 s (Fig. 3d). The change in the preferred strike direction is in favor of the existence of 3-D structures. Thus, it's better to employ 3-D MT inversion to obtain effective and reliable crustal electrical resistivity structures.

157
158 3.3 Inversion
159 As suggested by the above dimensionality analyses, 3-D modeling and inversion methods
160 are necessary. The 3-D inversion code ModEM (Egbert and Kelbert, 2012) was performed in this
161 study. The full impedance tensors (Z) at 22 equispaced periods in log domain in the range of
162 0.01 s to 1000.0 s were inverted. After 91 iterations, the preferred model was obtained with an
163 overall root-mean-square (RMS) misfit of 1.74. Qualitative comparisons of the fit of the
164 calculated responses to the observed estimates are shown by examining the apparent resistivity
165 and phase curves plotted in Figure 2 and S1. The preferred model in Figure 4 and S2 shows
166 major variations in the resistivity structures in the crust along the profile AA' and BB'
167 respectively. The sensitivity test results (Fig. S3) suggest the MT data could provide effective
168 constrains to the depth of 60 km.

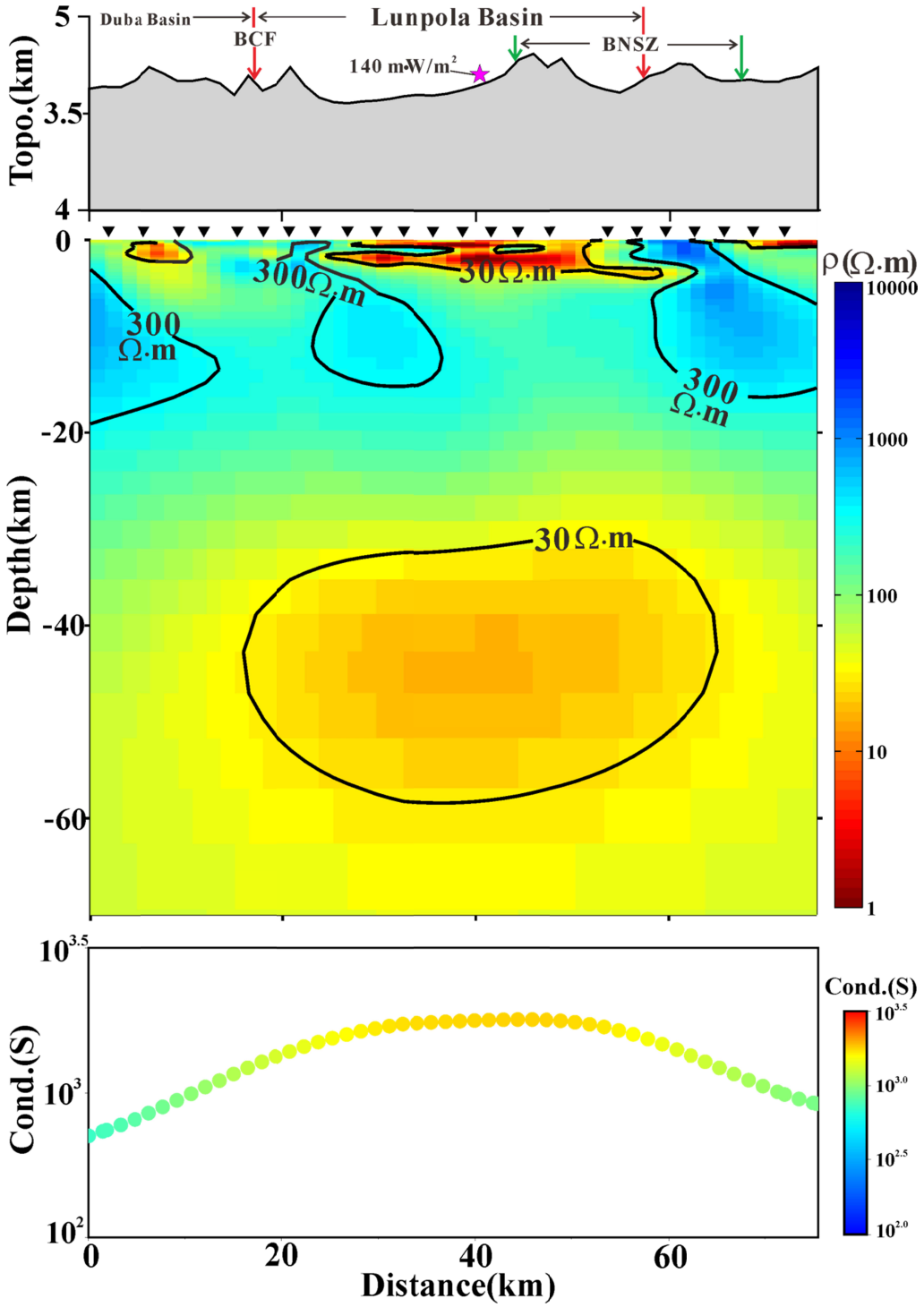

Figure 4. The preferred electrical resistivity model (a) along the profile AA', and the electrical conductance for the depth range of 30-60 km from the preferred model. The magenta star represents the heat flow measurement with 140m·W/m^2 (Jin et al., 2019).

4 Result and Discussion

4.1 Structure of Upper Crust

In the preferred 3-D inversion model (Fig. 4 and S2), the first-order electrical structures along the N-S profile are mainly composed of two contrasting layers that the resistive upper crust (≤ ~20 km) is underlain by the significantly low-resistivity middle and lower crust (~30-60 km). Within the upper crust, three prominent conductive zones (Fig. 4) are observed near the surface, which correlate spatially with the Duba basin at the southern transect, Lunpola basin in the central and topographic depression at the northern end, respectively. These discrete conductors in the upper crust are also observed in the previous results of the neighboring regions (Wei et al., 2001; Solon et al., 2005), and are confined to the low-velocity surficial layer defined in the wide-angle experiment (Zhao et al., 2001). Beneath the conductive surface layer, resistivities increase rapidly to hundreds of ohm meters.

The conductive surface zones are commonly believed to be associated with Mesozoic basin sediments overlain by Tertiary cover (Solon et al., 2005; Heinson et al., 2006). It's reasonable that the enhanced porosity of the basin should increase its conductivity, and resistivity variations within the sediments along the profile would be attributed to porosity differences and rock mineral compositions (Unsworth et al., 2004; Solon et al., 2005; Heinson et al., 2006). Beneath the Lunpola basin and nearby basins, the Cenozoic cover with low resistivities of 1-30 Ω·m is at least about 5000 m thick in a depocenter, which are in accord with the geological and drilling data (Wu et al., 2016). When the subsurface fluids (aqueous fluid or partial melting) form a well interconnected network and significantly decrease the resistivity, the content of deep fluids can be quantitatively estimated using the Archie's law (Unsworth et al., 2004, 2005; Bai et al., 2010; Dong et al., 2020). In the center of the Lunpola basin, the saline fluid fraction of 7.4-16.8% can explain the average sedimentary resistivity of about 2.0 Ω·m (Fig. S4).

4.2 Mid-to-lower Crustal Feature

In the preferred model (Fig. 4 and S2), the dominant feature is the conductive mid-to-lower crust. The sensitivity test shows the conductive anomaly in the middle and lower crust is robust (Fig. S3). We integrate the conductivities with depth to obtain conductance for the depth range of 20-60 km from the preferred model (Fig. 4B). The maximum conductance is about 2000 S beneath the Lunpola basin and the bulk resistivity is 20 Ω·m. As the anomalously low resistivity of the mid-to-lower crust in Tibet is a ubiquitous phenomenon which transect the whole plateau and its periphery (Wei et al., 2001; Solon et al., 2005; Unsworth et al., 2004, 2005; Dong et al., 2020; Xue et al., 2021), we believe the conductive anomaly in middle and lower crust beneath our profile must be the result of interconnected melt and/or aqueous fluids developed during the plateau's evolution. Using the Archie's law, the melt fraction is estimated in the range 1.3-3.0% for the bulk resistivity of 20 Ω·m beneath the Lunpola basin (Fig. S4).

In southern Tibet anatectic crustal melts and metamorphic brines generated as a consequence of underthrusting Indian crust and crustal thickening are the most likely candidates (Nabelek et al., 2009; Dong et al., 2020; Xue et al., 2021). However the northern limit of the underplated crust of the Indian plate is approximately parallel to about 30°N (Li et al., 2008; Nabelek et al., 2009; Xue et al., 2021) which is far away from the Lunpola Basin. In northern Tibet, the upper mantle is characterized by inefficient S-wave (Sn) propagation, low P-wave (Pn) velocity and strongly developed shear-wave anisotropy which indicates a hot anomalous mantle (Huang et al., 2000; Owens and Zandt, 1997). The partially melted mid-to-lower crust beneath the northern plateau is suggested be attributed to high temperatures (Owens and Zandt, 1997; Solon et al., 2005). The influx of heat from the hot underlying upper mantle or mantle derived melts injecting into the lower crust is a major influence on the development of this anomalous

crustal structure (Owens and Zandt, 1997; Huang et al., 2000; Solon et al., 2005). The Lunpola basin is within or near the southernmost edge of a region of high Sn attenuation and low upper mantle velocities. Therefore the hot upper mantle is suggested to blame for the partially melted mid-to-lower crust beneath the Lunpola basin. The high heat flow (140 m·W/m^2) (Fig. 1 and 4) (Jin et al., 2019) measured in the Lunpola basin favors the presence of the hot resource.

Compared to high electrical conductivities (~0.3 S/m) in mid-to-lower crust in the southern Tibet (Unsworth et al., 2005; Chen et al., 2018; Xue et al., 2021, 2022), the bulk conductivity (0.05 S/m) in mid-to-lower crust beneath the Lunpola baisn is clearly lower and analogous to the observed conductivities (~0.067 S/m) near the Karakorum strike-slip fault zone in the north-western Himalaya (Unsworth et al., 2005; Arora et al., 2007; Chen et al., 2018). The bulk conductivity of ~0.3 S/m requires a melt fraction of 5-14% which is sufficient to produce an order-of-magnitude reduction in viscosity, while the bulk conductivity of ~0.05-0.067 S/m requires a melt fraction of 1.3-4% that correspond to a more modest reduction in viscosity and a less-well-developed crustal flow (Unsworth et al., 2005). Chen et al. (2018) suggested the variation in bulk conductivity and melt fraction beneath the north-western Himalaya and the southern Tibet is attributed to fluid-absent melting and fluid-present melting respectively. The fluid-absent melting in mid-to-lower crust beneath the Lunpola basin in turn demonstrates the termination of the northward underthrusting Indian crust near 30°N (Li et al., 2008; Nabelek et al., 2009; Xue et al., 2021) which can provide sufficient fluids. Besides, the changes in crustal resistivity from south to north are also consistent with the changes in crustal velocity and Poisson's ratios which may be associated with the differences in upper-mantle structure and properties (Owen and Zandt, 1997; Huang et al., 2000).

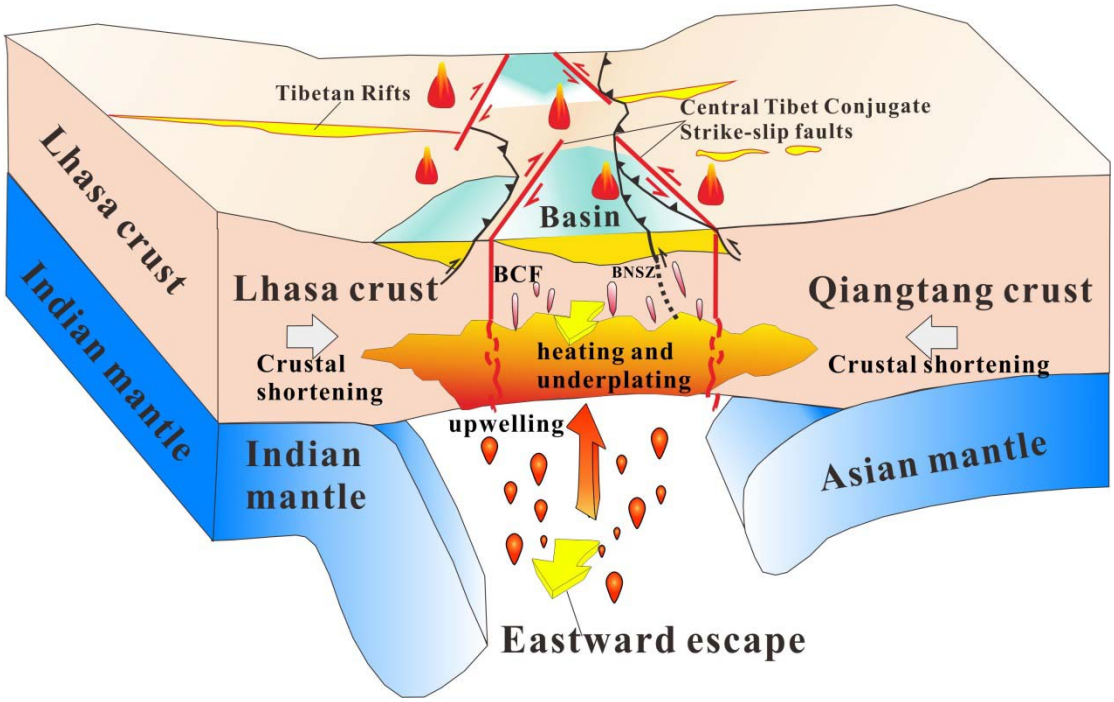

Figure 5 Interpretive cartoon illustrating the crustal deformation and underlying geodynamic processes beneath the central Tibet. Underthrusting of the Indian and Asian mantle lithosphere caused north-south contraction of the hot and softer asthenospheric channel, resulting in eastward asthenospheric flow and upwelling. Horizontal shear applied at the base could have driven the eastward escape of the central Tibet. The asthenospheric upwelling could induce basaltic underplating and thermally weaken the crust.

4.3 Eastward Escape of central Tibet

For the crustal deformation mechanisms and geodynamic processes in the central part of the Tibetan Plateau, Yin and Taylor (2011) proposed that the eastward asthenospheric flow along the BNSZ sandwiched between the cold Indian and Asian lithosphere applies horizontal shear at the base of the Tibetan mantle lithosphere to drive Cenozoic deformation of central Tibet. Recently based on paleotemperatures from the Lunpola Baisn, Xiong et al. (2022) proposed that mantle upwelling, immediate basaltic underplating and crustal shortening together contributed to the rise of the central Tibetan Valley. A number of evidences support a hot upper mantle in central Tibet and vertically coherent deformation of lithosphere of central Tibet (Owens and Zandt, 1997; Huang et al., 2000; Yin and Taylor, 2011). As discussed in section 4.2, the heating effect from the hot mantle would thermally weaken the crust characterized by low-resistivity anomalies (Fig. 4) and promote the crustal deformation. Nevertheless the relatively weak mid-to-lower crust beneath the Lunpola Basin is not enough to decouple the upper crust from the lower crust and the mantle lithosphere, which supports the crust and mantle lithosphere are deformed in a coherent fashion.

Our concept of the geodynamic processes driving late Cenozoic deformation of central Tibet is summarized in Fig. 5. In the model, underthrusting of the Indian and Asian mantle lithosphere caused north-south contraction of the hot and softer asthenospheric channel, resulting in eastward asthenospheric flow and upwelling. The basal shear at the base of the Tibetan lithosphere due to the asthenospheric flow, induces lateral motion of regional portions of the continental lithosphere bounded by conjugate strike-slip faults in central Tibet in a rigid block fashion (Yin and Taylor, 2011). Meanwhile, the asthenospheric upwelling could contribute to basaltic underplating and thermally weakening the crust, which promote crustal shortening and deformation, and rapid surface uplift of the central Tibet (Xiong et al., 2022).

5 Conclusions

In central Tibet, a series of Cenozoic basins along the Bangong-Nujiang suture are formed, and record the tectonic deformation and plateau growth responding to the collision of India and Asia. To study how the basins formed and the underlying geodynamic processes, magnetotelluric data across the Lunpola basin were collected to reveal the crustal structures beneath the basin and nearby area. Phase tensor analysis and 3-D inversions are performed to obtain the electrical resistivity model. The preferred model shows that the resistive upper crust inlaid with three surface conductive zones, is underlain by the significantly conductive middle and lower crust. The surface conductive zones correlate spatially with the basins and indicate the thick sedimentary sequences. The low-resistivity mid-to-lower crust is believed to be the result of partial melting, which may be attributed to fluid-absent melting induced by heat from the hot underlying upper mantle. The maximum conductance for the mid-to-lower is 2000 S with the bulk resistivity of 20 Ω·m, and the estimated fluid fraction is 1.3-3.0%. Compared to the significant weak mid-to-lower crust in southern Tibet, the crustal rheology is less well developed beneath central Tibet and not enough to decouple vertically from the mantle lithosphere. Combined with the previous studies in central Tibet, we suggest the crust and the mantle lithosphere are deformed in a coherent fashion, and propose that the hot asthenosphere beneath the central Tibet sandwiched between the cold Indian and Asian lithosphere, is squeezed to flow

eastward and upwells, resulting in the relatively weak mid-to-lower crust and driving the eastward escape of the continental lithosphere in central Tibet.

Acknowledgments

This study is supported by the National Natural Science Foundation of China (Grants 42174094), the Second Tibetan Plateau Scientific Expedition and Research Program (STEP) (Grant No. 2019QZKK0701-02), the National Key R&D Program of China (2022YFF0800900), and the Fund of Chinese Geological Survey (Grant No. DD20221647). The 3-D inversion code ModEM developed by Gary E. Egbert and Anna Kelbert (2012) is used.

Data Availability Statement

Inversion data files for the Magnetotelluric array study on the deep geo-electrical and rheological structure of the crust structure underneath the Lunpola basin beneath the central Tibet, was conducted by Institute of Geology, Chinese Academy of Geological Sciences in Beijing. The inversion data sets including the Magnetotelluric data and the model file used in this study are temporarily available in the "Data File(s) for Peer Review." If the paper is accepted for publication, the data will be archived at a FAIR compliant repository. The Kelbert et al., 2014 paper (https://doi.org/10.1016/j.cageo.2014.01.010) are recommended to refer for a brief understanding of the model and transfer function data file formats.

References

Armijo, R., P. Tapponnier, T. Han (1989), Late Cenozoic right-lateral strike-slip faulting in southern Tibet. *J. Geophys. Res.-Solid Earth and Planets*, 94 (B3): 2787-2838.

Arora, B. R., M. J. Unsworth, and G. Rawat (2007), Deep resistivity structure of the northwest Indian Himalaya and its tectonic implications. *Geophys. Res. Lett.*, 34: L04307.

Bai, D. H., M. J. Unsworth, M. A. Meju, X. B. Ma, J. W. Teng, X. R. Kong, Y. Sun, J. Sun, L. F. Wang, C. S. Jiang, C. P. Zhao, P. F. Xiao, and M. Liu (2010), Crustal deformation of the eastern Tibetan plateau revealed by magnetotelluric imaging. *Nature Geoscience*, 3 (5): 358-362.

Booker, J. R. (2014), The Magnetotelluric Phase Tensor: A Critical Review. *Surv. Geophys.*, 35 (1): 7-40.

Caldwell, T. G., H. M. Bibby, and C. Brown (2004), The magnetotelluric phase tensor. *Geophys. J. Int.*, 158 (2): 457-469.

Egbert, G. D., and A. Kelbert (2012), Computational recipes for electromagnetic inverse problems. *Geophy. J. Int.*, 189 (1): 251-267.

Egbert, G. D. (1997), Robust multiple-station magnetotelluric data processing. *Geophys. J. Int.*, 130 (2): 475-496.

Li, C., R. D. van der Hilst, A. S. Meltzer, and E. R. Engdahl (2008), Subduction of the Indian lithosphere beneath the Tibetan Plateau and Burma. *Earth Planet. Sci. Lett.*, 274 (1-2): 157-168.

Liang, H. D., S. Jin, W. B. Wei, R. Gao, G. F. Ye, L. T. Zhang, Y. T. Yin, and Z. W. Lu (2018), Lithospheric electrical structure of the middle Lhasa terrane in the south Tibetan plateau. *Tectonophysics*, 731-732: 95-103.

Nabelek, J., G. Hetenyi, J. Vergne, S. Sapkota, B. Kafle, M. Jiang, H. P. Su, J. Chen, B. S. Huang, and the Hi-CLIMB Team (2009), Underplating in the Himalaya-Tibet Collision Zone Revealed by the Hi-CLIMB Experiment. *Science*, 325 (5946): 1371-1374.

Owens, T. J., G. Zandt (1997), Implications of crustal property variations for models of Tibetan plateau evolution. *Nature*, 387 (6628): 37-43.

Solon, K. D., A. G. Jones, K. D. Nelson, M. J. Unsworth, W. F. Kidd, W. Wei, H. Tan, S. Jin, M. Deng, J. R. Booker, S. Li, and P. Bedrosian (2005), Structure of the crust in the vicinity of the Banggong-Nujiang suture in central Tibet from INDEPTH magnetotelluric data. *J. Geophys. Res.-Solid Earth*, 110 (B10): 1-20.

Tapponnier, P., Z. Q. Xu, F. Roger, B. Meyer, N. Arnaud, G. Wittlinger, and J. S. Yang (2001), Oblique Stepwise Rise and Growth of the Tibet Plateau. *Science*, 294 (5547): 1671-1677.

Unsworth, M. J., A. G. Jones, W. Wei, G. Marquis, S. G. Gokarn, J. E. Spratt, and the INDEPTH-MT team (2005), Crustal rheology of the Himalaya and Southern Tibet inferred from magnetotelluric data. *Nature*, 438 (7064): 78-81.

Unsworth, M. J., W. Wei, A. G. Jones, S. H. Li, P. Bedrosian, J. Booker, J. Sheng, D. Ming, and H. D. Tan (2004), Crustal and upper mantle structure of northern Tibet imaged with magnetotelluric data. *J. Geophys. Res.-Solid Earth*, 109 (B2).

Wei, W. B., M. J. Unsworth, A. Jones, J. Booker, H. D. Tan, D. Nelson, L. S. Chen, S. H. Li, K. Solon, P. Bedrosian, S. Jin, M. Deng, J. Ledo, D. Kay, and B. Roberts (2001), Detection of widespread fluids in the Tibetan crust by magnetotelluric studies. Science, 292 (5517): 716-718.

Wu, Z. H., Q. C. Zhang, Y. J. Wu, and P. S. Ye (2016), Response of sedimentary depression to crustal thickening in the Silin Co Basin and its adjacent area, Tibet. *Acta Geol. Sinica*, 90(9): 2181-2191 (in Chinese with abstract in English).

Yin, A., and M. H. Taylor (2011), Mechanics of V-shaped conjugate strike-slip faults and the corresponding continuum mode of continental deformation. *Geol. Soc. America Bull.*, 123 (9-10): 1798-1821.

Yin, A. (2000), Mode of Cenozoic east-west extension in Tibet suggesting a common origin of rifts in Asia during the Indo-Asian collision. *J. Geophys. Res*., 105 (B9): 21745-21759.

Chen, J. Y., F. Gaillard, A. Villaros, X. S. Yang, M. Laumonier, L. Jolivet, M. Unsworth, L. Hashim, B. Scaillet, and G. Richard (2018), Melting conditions in the modern Tibetan crust since the Miocene. *Nat. Commun.*, 9(1): 1-13

Dong, H., W. B. Wei, S. Jin, G. F. Ye, A. G. Jones, L. T. Zhang, J. E. Jing, C. L. Xie, and Y. T. Yin (2020), Shaping the Surface Deformation of Central and South Tibetan Plateau: Insights from Magnetotelluric Array Data. *J. Geophys. Res.-Solid Earth*, 125.

Fang, X. M., G. Dupont-Nivet, C. S. Wang, C. H. Song, Q. Q. Meng, W. L. Zhang, J. S. Nie, T. Zhang, Z. Q. Mao, and Y. Chen (2020), Revised chronology of central Tibet uplift (Lunpola Basin). *Sci. Adv.*, 6: eaba7298.

Heinson, G. S., N. G. Direen, and R. M. Gill (2006), Magnetotelluric evidence for a deep-crustal mineralizing system beneath the Olympic Dam iron oxide copper-gold deposit, southern Australia. *Geology*, 34(7): 573-576.

Huang, W. C., J. F. Ni, F. Tilmann, D. Nelson, J. R. Guo, W. J. Zhao, J. Mechie, R. Kind, J. Saul, R. Rapine, and T. M. Hearn (2000), Seismic polarization anisotropy beneath the central Tibetan Plateau. *J. Geophy. Res.*, 105(B12): 27979-27989.

Kapp, P., A. Yin, T. M. Harrison, and L. Ding (2005), Cretaceous-Tertiary shortening, basin development, and volcanism in central Tibet. *Geol. Soc. America Bull.*, 117(7/8): 865-878.

Rowley, D. B., and B. S. Currie (2006), Palaeo-altimetry of the late Eocene to Miocene Lunpola basin, central Tibet. *Nature*, 439: 677-681.

Su, T., A. Farnsworth, R. A. Spicer, J. Huang, F. X. Wu, J. Liu, S. F. Li, Y. W. Xing, Y. J. Huang, W. Y. D. Deng, H. Tang, C. L. Xu, F. Zhao, G. Srivastava, P. J. Valdes, T. Deng, and Z. K. Zhou (2019), No high Tibetan Plateau until the Neogene. *Sci. Adv.*, 5(3): eaav2189.

Wang, C. S., J. E. Dai, X. X. Zhao, Y. L. Li, S. A. Graham, D. F. He, B. Ran, and J. Meng (2014), Outward-growth of the Tibetan Plateau during the Cenozoic: A review. *Tectonophysics*, 621: 1-43.

Xiong, Z. Y., X. H. Liu, L. Ding, and A. Farnsworth (2022), The rise and demise of the Paleogene Central Tibetan Valley. *Sci. Adv.*, 8: eabj0944.

Xue, S., Z. W. Lu, W. H. Li, H. D. Liang, G. W. Wang, H. Y. Wang, H. Q. Li, and X. Li (2022), Three-dimensional electrical resistivity structure beneath the Cuonadong dome in the Northern Himalayas revealed by magnetotelluric data and its implication. *Sci. China Earth Sci.*, 65(8): 1538–1553.

Xue, S., Y. Chen, H. D. Liang, X. Li, X. F. Liang, X. B. Ma, Z. W. Lu, D. H. Bai, and Y. L. Yan (2021), Deep electrical resistivity structure across the Gyaring Co Fault in Central Tibet revealed by magnetotelluric data and its implication. *Tectonophysics*, 809

Zhao, W., J. Mechie, L. D. Brown, J. Guo, S. Haines, T. Hearn, S. L. Klemperer, Y. S. Ma, R. Meissner, K. D. Nelson, J. F. Ni, P. Pananont, R. Rapine, A. Ross, and J. Saul (2001), Crustal structure of central Tibet as derived from project INDEPTH wide-angle seismic data. *Geophys. J. Int.*, 145: 486-498.

391 Jin, C. S., X. G. Fu, W. B. Chen, D. W. Qaio, J. Ge, Y. H. Zhu, Z. Q. Lu, and P. K. Lu (2019), Measurements of
392 borehole heat flow in northern Tibet. *Chinese J. Geophys.*, 62(8): 3095-3105. (in Chinese with abstract in
393 English).